Characteristics of Radiating Variable Resonant Frequency Crystal Systems*

WALTER WELKOWITZ AND WILLIAM J. FRY
Bioacoustics Laboratory, University of Illinois, Urbana, Illinois
(Received October 30, 1953)

Calculations based on the usual one-dimensional theory of piezoelectric crystal systems have been carried out for several particular variable resonant frequency crystal systems radiating into water. Curves are presented showing the (1) power output as a function of frequency for operation both on and off resonance, (2) resonant frequency shift as a function of backing length, and (3) relative band width as a function of frequency. The validity of certain approximations is checked so that the operating characteristics of systems made up of different materials can be quickly estimated. The curves indicate that a variable resonant frequency system of crystals all of equal free-free resonant frequency operating with an allowable power variation for fixed applied field strength of 2:1 can have a continuous variation of resonant frequency of about 2.3:1. A system half the crystals of which have twice the free-free resonant frequency of the others for the same allowable field strength variation can operate over a frequency range of about 5.3:1.

INTRODUCTION

STARTING with some experimental observations by Fox and Rock[1] on the possibilities of shifting the resonant frequency of a crystal by loading, the development of variable resonant frequency transducers has progressed to the point where high-power transducers operating in this manner are practical. Papers by Fry, Fry and Hall,[2] and by Hall and Fry[3] have covered the problem of designing and constructing a suitable backing chamber, so that the backing material used to shift the crystal frequency (in their case mercury) is properly coupled to the crystal, is decoupled from the chamber walls, and is of a suitable geometry to shift the frequency as desired. The theoretical aspects of this previous work considered the crystal system under nonradiating conditions while the experimental work dealt with both nonradiating and radiating situations.

It is the purpose of this paper to consider from the viewpoint of the usual one-dimensional theory of piezoelectric crystal systems[4] some of the characteristics of such systems under radiating conditions. The characteristics investigated are power output as a function of frequency for operation both on and off resonance, resonant frequency shift as a function of backing length, and relative band width (the reciprocal of Q) as a function of resonant frequency. Curves of these properties of the crystal system are presented for a number of harmonics as well as for the fundamental frequency, since both theoretical and experimental work demonstrate that under certain conditions, operation on harmonics is to be preferred over operation on the fundamental frequency.

Fry, Fry, and Hall[2] analyzed the mercury backing on the basis of a three-dimensional theory. With respect to the range of applicability of a one-dimensional theory, a consideration of their work indicates that the effects of the more complex theory show up mainly in the calculated length of mercury backing required to shift the frequency to any given operating point and in the design criteria to keep losses low. For situations where the cross-sectional dimensions are large compared to the wavelength and the system is lossless, the more complex analysis reduces to the lossless one-dimensional theory analysis used herein. The present investigation assumes that losses in the backing are negligible compared to the power radiated. Some objections to the use of a one-dimensional theory are suggested by the experimental investigations. It appears that interference from various modes of vibration in the crystal enter the picture. Shear waves in the liquid medium used to surround the crystals and to couple them to the water into which they radiate are of importance in determining the efficiency of the transducers. These problems are beyond the scope of this paper.

The extensive numerical work required for the curves was carried out on the Ordvac digital computer, and while it is felt that such an instrument is a powerful tool for use in solving complex acoustical problems, it is considered desirable where possible to indicate approximations that are valid as checked by the computer so that useful results can be obtained by rapid hand computation. With this in mind, a study of the calculations and curves indicated that the equation for the curve of power output as a function of resonant frequency can be quite accurately derived for systems of the type considered herein, under the assumption that the frequency of operation is not shifted by the radiation loading. This assumption appears to be valid for all commonly used crystal and ceramic transducer materials radiating directly into water. Furthermore, the shape of the desired curve is the same for all such materials under this assumption. Only changes of scale occur and these are a natural result of the different acoustic impedances involved. This curve is therefore applicable to all reactively loaded crystal and ceramic systems radiating directly into water.

* This work was supported by the Bureau of Ships under Contract Nobsr-52367.

[1] F. E. Fox and G. D. Rock, Proc. Inst. Radio Engrs. **30**, 29 (1942).

[2] Fry, Fry, and Hall, J. Acoust. Soc. Am. **23**, 94 (1951).

[3] W. L. Hall and W. J. Fry, Rev. Sci. Instr. **22**, 155 (1951).

[4] See for example Fry, Taylor, and Henvis, *Design of Crystal Vibrating Systems* (Dover Publications, Inc., New York, 1948).

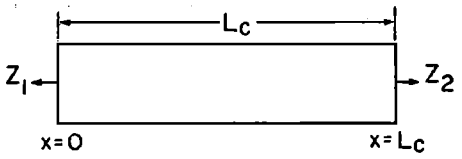

FIG. 1. Diagram of the crystal for theoretical consideration.

The transducer materials considered in the calculations are the commonly used ammonium dihydrogen phosphate 45° Z-cut crystal (hereafter referred to as ADP) and the more recently developed barium titanate ceramic. The latter was analyzed operating in thickness mode, but simplified equations which are identical in form to those resulting from longitudinal mode operation analysis were used, and therefore the only differences in calculated values for longitudinal mode operation of the ceramic will be the result of numerical differences in some of the constants. For the ADP case, backings of mercury and steel were considered so that a comparison could be made between continuously variable systems and commonly used fixed frequency systems. In the case of the barium titanate only mercury backing was considered in the calculations. In all cases the transducer was studied under the condition of radiation into water. It was assumed that the water appeared as a purely resistive load to the crystal. This is approximately the case when the diameter of the radiating face is large compared to the wavelength.[5]

NOTATION

A: cross-sectional area of crystal system.
$B_1 = \frac{1}{2}(3N_2+N_1^2N_2)$.
$B_2 = -2N_2$.
$B_3 = \frac{1}{2}(N_2-N_1^2N_2)$.
$B_4 = \frac{1}{2}(3N_2-N_1^2N_2)$.
$B_5 = -(N_2+N_1N_2)$.
$B_6 = (N_1N_2-N_2)$.
$B_7 = \frac{1}{4}(N_2+2N_1N_2+N_1^2N_2)$.
$B_8 = \frac{1}{4}(N_2-2N_1N_2+N_1^2N_2)$.
$B_9 = \frac{1}{2}(N_2^2+N_1^2+N_1^2N_2^2+1)$.
$B_{10} = \frac{1}{2}(N_2^2+N_1^2-N_1^2N_2^2-1)$.
$B_{11} = \frac{1}{2}(N_2^2-N_1^2-N_1^2N_2^2+1)$.
$B_{12} = \frac{1}{4}(N_2^2-N_1^2+N_1^2N_2^2+2N_1N_2^2-2N_1-1)$.
$B_{13} = \frac{1}{4}(N_2^2-N_1^2+N_1^2N_2^2-2N_1N_2^2+2N_1-1)$.
C_0: Clamped capacity of the crystal system.
d: Piezoelectric constant: d_{21} for the longitudinal mode case, $(-e_{11}/C_{11}^E)$ for the thickness mode case, notation as in reference 4.
E: voltage applied to the crystal system.
f: frequency.
$_0$: fundamental resonant frequency of the free crystal.
L_c: length of the crystal.
l_t: thickness of the crystal.
L_1: length of the backing material.
$N_1 = \rho_1 V_1/\rho_c V_c$.
$N_2 = \rho_2 V_2/\rho_c V_c$.
P: total power output of the crystal system.
$Q = \beta/\Delta\beta = f_0/\Delta f$.
s: elastic constant: S_{11}^E for the longitudinal mode case, $1/C_{11}^E$ for the thickness mode case, notation as in reference 4.
V_c: velocity of sound in the crystal.
V_1: velocity of sound in the backing material.
V_2: velocity of sound in the loading material (water).
Z_e: electrical input impedance of the crystal system.
Z_1: mechanical impedance of the backing.
Z_2: mechanical impedance of the load.
Z_0: mechanical impedance of the crystal. $Z_0 = A\rho_c V_c$.
$\alpha = L_1/L_c$.
$\beta = f/f_0$.
$\Delta\beta/\beta = \Delta f/f_0$, where Δf is the bandwidth at the half-power point.
$\gamma_c = \omega L_c/V_c = \pi\beta$.
$\gamma_1 = \omega L_1/V_1 = \pi(V_c/V_1)\alpha\beta$.
ρ_c: density of the crystal material.
ρ_1: density of the backing material.
ρ_2: density of the loading material.
$\varphi = (d/s)(A/L_c)$ for thickness mode operation.
$= (d/s)(A/l_t)$ for longitudinal mode operation.
$\omega = 2\pi f$.

THEORY

Consider a crystal loaded at both ends as indicated in Fig. 1. The electrical input impedance for such a system is given by[4]

$$Z_e = 1/(j\omega C_0 + \varphi^2 M), \tag{1}$$

where

$$M = \frac{-2(1-\cos\gamma_c)+j\left(\frac{Z_1}{Z_0}+\frac{Z_2}{Z_0}\right)\sin\gamma_c}{Z_0\left[\left(\frac{Z_1}{Z_0}+\frac{Z_2}{Z_0}\right)\cos\gamma_c+j\left(\frac{Z_1}{Z_0}\cdot\frac{Z_2}{Z_0}+1\right)\sin\gamma_c\right]}. \tag{2}$$

As shown in Fig. 2 this impedance is equivalent to that of an electrical circuit of a condenser in parallel with a complex admittance equal to $\varphi^2 M$. In accordance with the previous assumptions concerning the backing system and the radiation load, the impedance of the

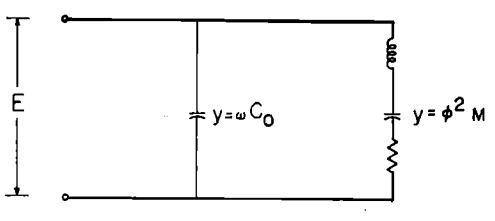

FIG. 2. Equivalent electrical circuit for the crystal system.

[5] See for example P. M. Morse, *Vibration and Sound* (McGraw-Hill Book Company, Inc., New York, 1948).

backing can be represented by

$$Z_1 = jA\rho_1 V_1 \tan\gamma_1, \tag{3}$$

while the load can be represented adequately by a purely resistive impedance of the form

$$Z_2 = A\rho_2 V_2. \tag{4}$$

Since it is convenient to work with the ratios of the characteristic impedances of the various media involved, we define N_1 and N_2 as follows:

$$N_1 = \rho_1 V_1 / \rho_c V_c$$

and

$$N_2 = \rho_2 V_2 / \rho_c V_c.$$

Combining Eqs. (2), (3), and (4),

$$M = \frac{-2 + 2\cos\gamma_c - N_1 \sin\gamma_c \tan\gamma_1 + jN_2 \sin\gamma_c}{Z_0[N_2 \cos\gamma_c - N_1 N_2 \sin\gamma_c \tan\gamma_1] + jZ_0[N_1 \cos\gamma_c \tan\gamma_1 + \sin\gamma_c]}. \tag{5}$$

From Fig. 2, it is apparent that the power input to the circuit is

$$P = E^2 \varphi^2 \, \mathrm{Re}M. \tag{6}$$

Since in this analysis the crystal and the backing are considered lossless, it follows that this is also the total acoustic power radiated by the system.

The expressions can be placed in dimensionless form by introducing the parameters defined as follows:

$$\beta = f/f_0$$

and

$$\alpha = L_1/L_c.$$

By suitable algebraic manipulation, Eq. (6) can be recast in the form

$$\left.\begin{matrix} \dfrac{Pl_t^2}{AE^2} \\ \dfrac{PL_c^2}{AE^2} \end{matrix}\right\} = \frac{\dfrac{(d/s)^2}{\rho_c V_c}\left[B_1 + B_2\cos\pi\beta + B_3\cos 2\pi\beta + B_4\cos 2\pi\frac{V_c}{V_1}\alpha\beta + B_5\cos\pi\beta\left(1+2\frac{V_c}{V_1}\alpha\right) + B_6\cos\pi\beta\left(1-2\frac{V_c}{V_1}\alpha\right) + B_7\cos 2\pi\beta\left(1+\frac{V_c}{V_1}\alpha\right) + B_8\cos 2\pi\beta\left(1-\frac{V_c}{V_1}\alpha\right)\right]}{B_9 + B_{10}\cos 2\pi\beta + B_{11}\cos 2\pi\frac{V_c}{V_1}\alpha\beta + B_{12}\cos 2\pi\beta\left(1+\frac{V_c}{V_1}\alpha\right) + B_{13}\cos 2\pi\beta\left(1-\frac{V_c}{V_1}\alpha\right)}. \tag{7}$$

The B_i's in this case are functions only of the impedance ratios N_1 and N_2. The choice of symbols on the left side of the equation depends upon whether longitudinal or thickness mode operation is being investigated. The upper set is used with the longitudinal mode calculations and the lower set with the thickness mode calculations.

All the computations are based on Eqs. (7). The procedure followed was to calculate values of (7), with the constants for specific materials inserted for thirty-six fixed values of α, and with β covering a sufficient number of values to completely define the resonant peaks. For the cases involving ADP, evaluations were performed for between 500 and 1000 values of β for each value of α. In the case of barium titanate the Q of the system radiating into water is much higher than for ADP, therefore, about ten times the point density was used. Figures 3, 4, 5, 6, 7, and 8 show some representative curves for the ADP-mercury and barium titanate-mercury systems. It is apparent from these curves that the Q of the barium titanate system is on the average about six times that of the ADP system. The ADP-steel curve is, of course, identical with the ADP-mercury curve for the case of no backing, but for

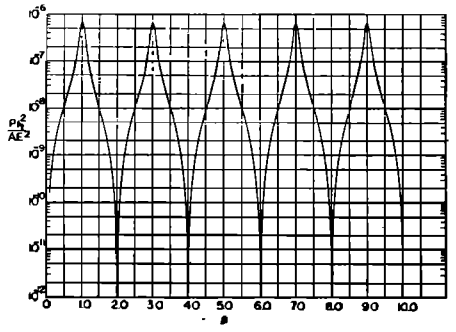

FIG. 3. Variation of the power output as a function of frequency of an ADP-mercury system radiating into water for the case of zero mercury backing.

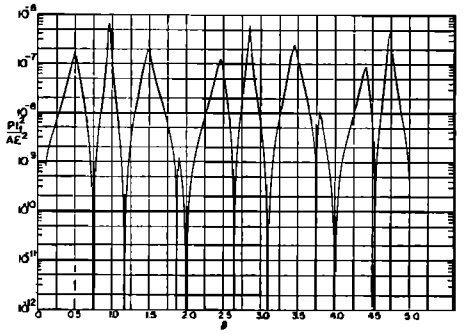

FIG. 4. Variation of the power output as a function of frequency of an ADP-mercury system radiating into water for the case of approximately quarter wave backing ($\alpha = 0.48$).

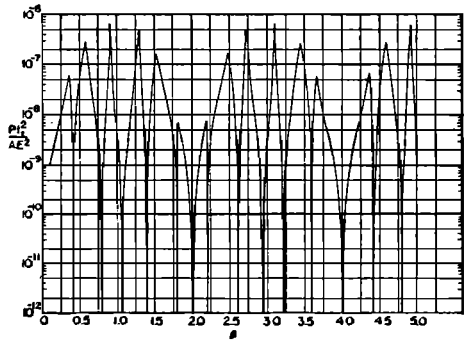

FIG. 5. Variation of the power output as a function of frequency of an ADP-mercury system radiating into water for the case $\alpha=1.00$.

other lengths of backing the band widths of the resonant peaks are different, although the peak values are the same.

From the curves of power output as a function of β for fixed values of α, all the other characteristic curves

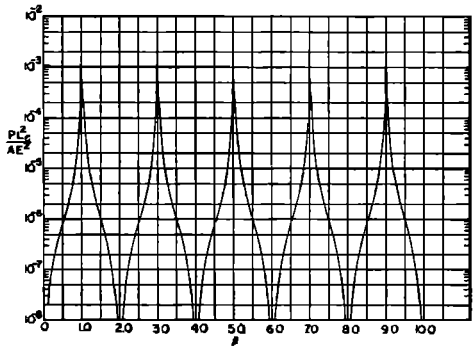

FIG. 6. Variation of the power output as a function of frequency of a barium titanate-mercury system radiating into water for the case of zero backing.

were derived. Figures 9, 10, and 11 are curves of frequency shift as a function of backing length for the three combinations of materials discussed. Examination of these curves indicates that the results are very closely approximated by the simple equation for resonance of a backed crystal not loaded on the opposite

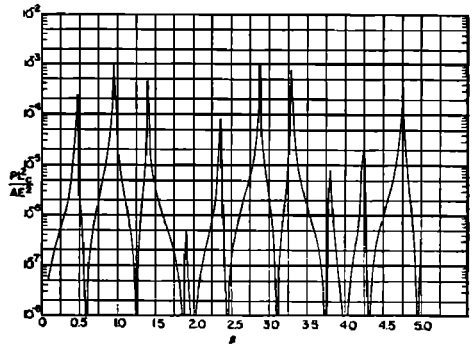

FIG. 7. Variation of the power output as a function of frequency of a barium titanate-mercury system radiating into water for the case of approximately quarter wave backing ($\alpha=0.32$).

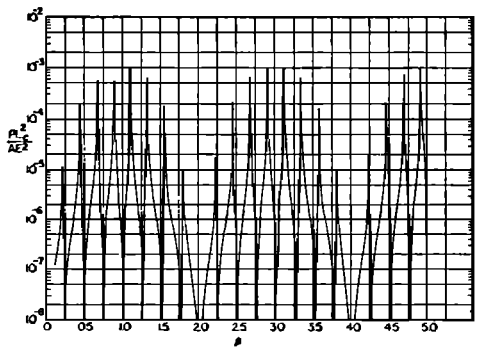

FIG. 8. Variation of the power output as a function of frequency of a barium titanate-mercury system radiating into water for the case $\alpha=1.00$.

end. This equation is

$$N_1 \tan\gamma_1 = -\tan\gamma_c. \tag{8}$$

By introducing the parameters α and β the following result is obtained from (8)

$$\alpha = (V_1/V_c\pi\beta)\tan^{-1}[(1/N_1)\tan\pi(n-\beta)]. \tag{9}$$

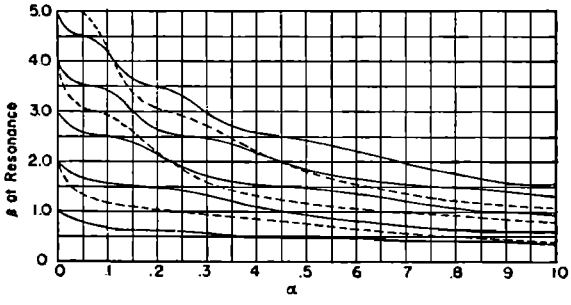

FIG. 9. Resonant frequency shift characteristic as a function of relative backing length for an ADP-mercury system. The dotted curves represent the loci of zeros that separate the resonant peaks. The lines $\beta=2n$ also represent loci of zero functions.

Figure 12 is a curve of relative power output as a function of resonant frequency. It is valid for all the combinations of materials analyzed. A straightforward analysis indicates that it is valid for any combination of materials for which the approximation of Eq. (8) is

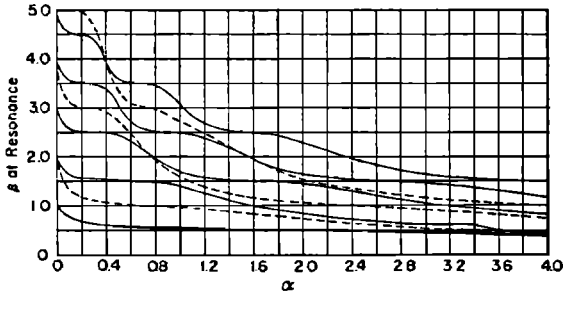

FIG. 10. Resonant frequency shift characteristic as a function of relative backing length for an ADP-steel system. The dotted curves represent the loci of zeros that separate the resonant peaks. The lines $\beta=2n$ also represent loci of zero functions.

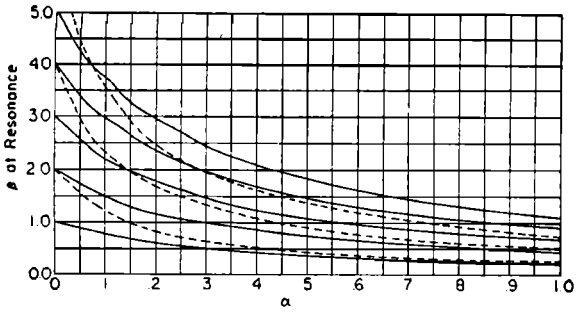

FIG. 11. Resonant frequency shift characteristic as a function of relative backing length for a barium titanate-mercury system. The dotted curves represent the loci of zeros that separate the resonant peaks. The lines $\beta = 2n$ also represent loci of zero functions.

valid. If Eqs. (5), (6), and (8) are combined

$$\left.\begin{matrix} \frac{Pl_i^2}{AE^2} \\ \frac{PL_c^2}{AE^2} \end{matrix}\right\} = \frac{(d/s)^2}{\rho_2 V_2}(\cos\gamma_c - 1)^2. \qquad (10)$$

TABLE I. Peak power output at resonance for unit area and field strength for various transducer materials.

Material	$\frac{4(d/s)^2}{\rho_2 V_2}$ mhos $(10)^6$
ADP, 45° Z-cut	0.680
Barium titanate (thickness mode)	1130.0
Rochelle salt, 45° Y-cut	0.264
Quartz, X-cut	0.087

From Eqs. (10) it can be seen that if numerical values of the power output for unit field strength and area are desired, values from the curve of Fig. 12 must be multiplied by $4(d/s)^2/\rho_2 V_2$. This multiplying constant is tabulated in Table I for a number of common transducer materials radiating into water.

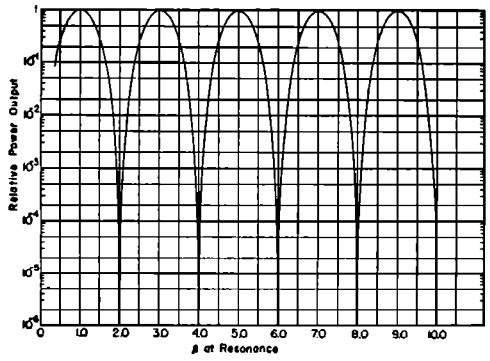

FIG. 12. Characteristic curve of relative power output as a function of resonant frequency. This curve is valid for all the systems investigated and most similar systems.

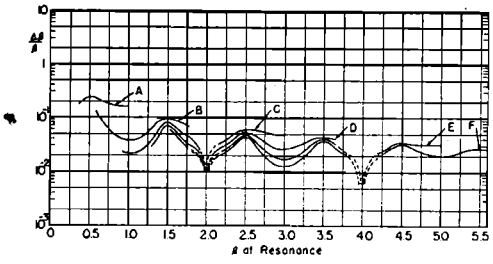

FIG. 13. Relative band width as a function of frequency for the ADP-mercury system radiating into water.

A—fundamental
B—2nd harmonic
C—3rd harmonic
D—4th harmonic
E—5th harmonic
F—6th harmonic.

Figures 13, 14, and 15 are curves of relative bandwidth for the various systems. No accurate and simple approximation method has been found, during the progress of the work reported here, for evaluating points on these curves. A comparison of the ADP-mercury and barium titanate-mercury curves indicates that the

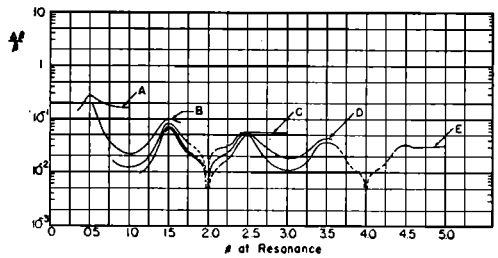

FIG. 14. Relative band width as a function of frequency for the ADP-steel system radiating into water.

A—fundamental
B—2nd harmonic
C—3rd harmonic
D—4th harmonic
E—5th harmonic.

band widths for the barium titanate system are about one-sixth of those for the AD Psystem. From these curves it will be noted that the relative band width approaches zero in the limit as β approaches 2 and 4. This is readily shown in the following manner.

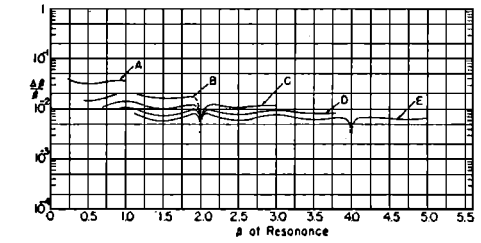

FIG. 15. Relative band width as a function of frequency for the barium titanate-mercury system radiating into water.

A—fundamental
B—2nd harmonic
C—3rd harmonic
D—4th harmonic
E—5th harmonic.

From Eq. (5) it follows that

$$\mathrm{Re}M=\frac{N_2(N_1\tan\gamma_1\sin\gamma_c-\cos\gamma_c+1)^2}{Z_0(N_2\cos\gamma_c-N_1N_2\sin\gamma_c\tan\gamma_1)^2+Z_0(N_1\cos\gamma_c\tan\gamma_1+\sin\gamma_c{}^2)}. \tag{11}$$

Therefore the curves of power output have zeros at

$$\gamma_c=2n\pi, \quad n=1, 2, \cdots \tag{12}$$

and

$$N_1\tan\gamma_1=(\cos\gamma_c-1)/\sin\gamma_c. \tag{13}$$

In the nondimensional notation, the loci of these zeros are given by

$$\beta=2n \tag{14}$$

and

$$\alpha=(V_1/V_c\pi\beta)\tan^{-1}[(1/N_1)(\cos\pi\beta^{-1})/\sin\pi\beta]+nV_1/\beta V_c. \tag{15}$$

Curves of these loci are shown on Figs. 9, 10, and 11 for the different systems under consideration. It is apparent from these curves that resonant peaks are always separated by zeros and that as $\beta\rightarrow 2, 4, 6\cdots$, the width of a peak curve as measured by the frequency difference between zeros approaches zero. It follows therefore that the band width, which is defined as the frequency difference at the half-power points also approaches zero as $\beta\rightarrow 2, 4, 6\cdots$, and the relative band width $(\Delta\beta/\beta)$ does the same.

DISCUSSION

In any attempt to utilize the information in this paper to design variable resonant frequency transducers, it would be of great value to know the range of validity of the curves which were derived from a simplified model theory. Since ADP-mercury variable resonant frequency transducers of this type have been constructed and tested, it is possible to compare theory and measurement. For a typical transducer, the following results were obtained. There is good agreement of the experimental results with theory for the frequency shift as a function of backing length for the fundamental and second harmonic. Measurements of relative band width as a function of resonant frequency agree in magnitude with the theory for the fundamental and second harmonic but the scatter of the measured points is, in this case, too great for a comparison of the shape of the curves. In this lossless analysis relative power output and relative input conductance represent the same property, but curves from the measured data for this transducer indicate that while there is good agreement with the theory for relative power output as a function of frequency, for operation on the fundamental and the second harmonic, the curve of relative input conductance, for second harmonic operation, differs from the theoretical curve. A more comprehensive theory is apparently needed in this situation.

TABLE II. Characteristic impedances of various materials.

Material	Characteristic impedance (ρV) $\frac{\text{Kg}}{\text{m}^2\,\text{sec}}$ $(10)^{-6}$
Steel	39.3
Mercury	19.8
Water	1.43
ADP, 45° Z-cut, longitudinal mode	5.90
Barium titanate, thickness mode	25.7

From previous theoretical and experimental work on crystal vibrating systems by numerous investigators, information is available on the dependence of the properties of such systems upon the impedances presented to the crystal. This paper extends this body of information. Table II contains the characteristic impedances of the various materials considered for ready reference. Figures 13, 14, and 15 illustrate the well-known dependence of the magnitude of the band width on the ratio of the characteristic impedances of the transducer material and water. For the ADP cases where the impedance match is better than for the barium titanate case, the magnitude of the band width is greater. Figures 9, 10, and 11 illustrate the smoothness with which the resonant frequency shifts as a function of the length of the backing material for various ratios of the characteristic impedances of the transducer material and the backing material. The barium titanate-mercury system is best, the ADP-steel system is poorest. The fluctuation of the relative band width is dependent upon this same impedance ratio. The barium titanate-mercury system shows the least fluctuation while the ADP-steel system shows the greatest. The locations of the maxima of the band width curves depend upon whether this impedance ratio is greater or less than one. Thus for the ADP systems, in which this impedance ratio is less than one, the maxima of the band-width curves are located at different relative frequencies than for the barium titanate system.

In the design and construction of an actual variable resonant frequency system, the choice of materials will naturally be highly dependent upon the application. For biological experimentation where output level stability is an important factor, quartz or ADP crystals might be preferred over barium titanate. Quartz in thickness mode operation is more suitable for high-frequency operation and ADP in longitudinal mode is more suitable for lower-frequency operation. For applications where it is desirable to keep the applied voltage as low as possible, barium titanate is a suitable material.

The advantage of a variable resonant frequency system over a fixed-backed (or air-backed) transducer system is that for a given allowable variation in power

at constant driving voltage, the continuous operating range of frequencies is much greater. For example if we can allow a variation in power output for fixed driving field strength of 2:1, then from Fig. 12 it appears that a continuous operating frequency range of about 2.3:1 is obtainable for the variable resonant frequency system. The corresponding figure for an ADP air-backed system directly coupled to water (Fig. 3) is 1.17:1, while for a barium titanate air-backed system directly coupled to water (Fig. 6) this figure is only 1.04:1. Thus far we have considered variable resonant frequency systems with crystals of only one free-free resonant frequency. If we consider a multiple element transducer with crystals of two free-free resonant frequencies in the ratio of two to one, then for the same allowable variation in power, operation over a continuous frequency range of about 5.3:1 is feasible as indicated in Fig. 16.

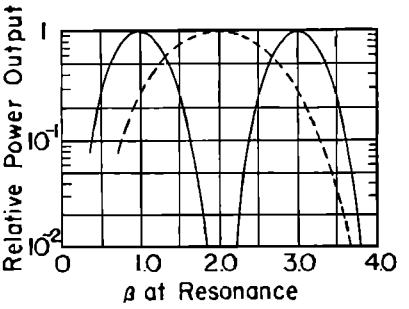

FIG. 16. Characteristic curve of relative power output as a function of resonant frequency for a multiple crystal system which has crystals of two free-free resonant frequencies in the ratio of two to one. The solid line represents the output of the lower frequency crystals while the dotted line represents the output of the higher frequency crystals. The two sets of crystals are considered to be independently driven.

CONCLUSIONS

Curves of the characteristics of frequency shift, band width, and output power of radiating variable resonant frequency systems have been presented. These curves are reasonably reproduced under experimental conditions and can therefore be used in a predictive capacity in designing transducers. For systems of crystals of one free-free resonant frequency, if a 2:1 variation in power output is allowable, a continuous frequency range of about 2.3:1 is readily attainable for resonant operation. For multiple crystal systems where crystals of two free-free resonant frequencies in the ratio of two to one are used, this frequency range can be increased to about 5.3:1.

ACKNOWLEDGMENT

We wish to thank Professor J. E. Robertson for coding the computations for the Ordvac digital computer, and Mr. C. W. Peterson for plotting the large number of curves.